

# Analytical model for determining effective stiffness and mechanical behavior of polymer matrix composite laminates using continuum damage mechanics

International Journal of Damage  
Mechanics

2020, Vol. 29(10) 1512–1542

© The Author(s) 2020

Article reuse guidelines:

sagepub.com/journals-permissions

DOI: 10.1177/1056789520939624

journals.sagepub.com/home/ijd



Sota Onodera<sup>1</sup>  and Tomonaga Okabe<sup>1,2</sup>

## Abstract

The present paper proposes a new analytical model for predicting the effective stiffness of composite laminates with fiber breaks and transverse cracks. The model is based on continuum damage mechanics and the classical laminate theory. We derived damage variables describing stiffness reduction due to fiber breaks and its maximum value during ultimate tensile failure from the global load-sharing model. Furthermore, a simplified analytical model is presented for obtaining two damage variables for a cracked ply subjected to transverse tensile loading or in-plane shear loading. This model was developed assuming that the displacement field of the longitudinal direction can be expressed in the form of a quadric function by loosening the boundary condition for the governing differential equation. For verifying the developed model, the elastic constants of damaged composite laminates were predicted for cross-ply and angle-ply laminates and compared with the finite element analysis results. As for the appropriate expression of the effective elastic stiffness matrix of the damaged ply, we verified four types of effective compliance/stiffness matrices including the Murakami, Yoshimura, Li, and Maimí models. We found the Maimí model to be the most appropriate among these four models. Moreover, we successfully simplified the expressions for damage variables in the complicated infinite series obtained in our previous study. We also proved that this could contribute toward improving the accuracy of our analysis. After verifying the present model, the stress–strain response and failure strength of carbon- or glass-fiber-reinforced plastic cross-ply laminates were predicted using Maimí’s compliance model and the simplified damage variables.

## Keywords

Transverse crack, continuum damage mechanics, damage variable, composite laminate, polymer matrix composite

<sup>1</sup>Department of Aerospace Engineering, Tohoku University, Miyagi, Japan

<sup>2</sup>Department of Materials Science and Engineering, University of Washington, Seattle, WA, USA

## Corresponding author:

Sota Onodera, Department of Aerospace Engineering, Tohoku University, 6-6-01, Aramaki Aza Aoba, Aoba-ku, Sendai, Miyagi 980-8579, Japan.

Email: sonodera@plum.mech.tohoku.ac.jp

## Introduction

The application scope of advanced composite materials is increasing due to their superior mechanical properties like high specific modulus and strength. The specific modulus plays an important role in real structures, but the specific strength of these materials has not been effectively utilized in real applications owing to the incapability of failure analysis. The reason why effective designs considering the high specific strength are not yet developed is that structural designs are developed using the strain criterion based on initial ply failure. When load is applied to composite structures, matrix cracks are generated in the transverse ply. However, if the applied strain level is low, these cracks do not cause secondary damage and affect the reduction of stiffness. Furthermore, if the applied strain reaches a certain level, the damage migrates from the ply cracks, leading to catastrophic damage phenomena like delamination and fiber breakage. Thus, similar to metals, if designers consider the initial damage and users can predict the progress of the damage, the structural weight can be reduced. Therefore, damage tolerance designing is the next step for expanding the application scope of composite structures.

Designers need to analyze the stiffness reduction in composite structures owing to transverse cracks accurately. Transverse cracks occurring in cross-ply laminates have been studied since the 1970s (Bailey and Parvizi, 1981; Garrett and Bailey, 1977a, 1977b; Manders et al., 1983; Parvizi and Bailey, 1978; Parvizi et al., 1978). Initially, there were many stress analysis studies performed using the shear-lag model, which was developed to analyze the stress profile around discontinuous fibers (Cox, 1952). Using the shear-lag model, the damage progress could be predicted using the stress criterion and/or energy criterion. Specifically, the onset of transverse cracks from the viewpoint of micromechanics was analyzed. In the 1980s, the shear-lag model was improved (Han et al., 1988; Lee and Daniel, 1990). Finite element analysis (FEA) (Wang et al., 1984) and the minimum energy principle model (Hashin, 1986, 1987; Lee et al., 1989) utilizing variation methods were proposed to analyze the stress field around the transverse cracks. These models enable us to calculate the stress field around the transverse cracks in cross-ply laminates very accurately.

In addition to the above approaches, continuous damage mechanics (CDM) models (Allen et al., 1987a, 1987b; Talreja, 1985) were developed simultaneously. CDM models are divided into the following two types: the first one involves the effective elastic stiffness or compliance matrix utilizing the damage tensor derived from the thermomechanical relationship, while the other one calculates the inelastic strain with internal state variables so that the average stress of the laminate can be estimated. Both models are fitted with the classical laminate theory (CLT) because the detailed stress distribution in the laminate is unnecessary, and the damaged ply is homogenized. Therefore, arbitrary laminates other than cross-ply laminates can be analyzed easily. On the contrary, problems regarding the objective determination of damage tensor and internal state variables must be addressed.

In 1992, McCartney presented an accurate anisotropic elastic solution for cross-ply laminates, satisfying both the equilibrium and compatible equation. Pagano et al. (1998) proposed an accurate solution based on cylindrical bending. Moreover, several researchers analyzed the delamination migrating from the matrix crack from the view point of energy balance (Nairn and Hu, 1992; Noda et al., 2004). Xia et al. (1993) used the McCartney model to analyze damage progress in ceramic-matrix cross-ply laminates. Furthermore, using CDM, Gudmundson and Zang (1993) extended the two-dimensional model of Dvorak et al. (1985, 1987) which is applicable to an isotropic body to obtain a three-dimensional model with the generalized laminate theory for analyzing three-dimensional laminates. As stated above, CDM can be applied to angle-ply laminates. Gudmundson and Zang (1993) applied the model to study stiffness reduction in angle-ply laminates. Kobayashi et al. (2000) used the Gudmundson and Zang (1993) model to predict the damage progress in

quasi-isotropic carbon-fiber-reinforced plastic (CFRP) laminates. After the 2000s, several researchers (Hajikazemi and McCartney, 2018; McCartney, 2017; Vinogradov and Hashin, 2010) continued to develop models for analyzing arbitrary laminates other than cross-ply laminates. However, the derived formulations are extremely complicated for ordinary people to use them easily.

Recently, we derived the analytical form of the damage tensor with transverse crack density by solving the Laplace equation for the displacement fields under the generalized plane strain condition (Okabe et al., 2018). The laminate stiffness can be estimated with the obtained damage tensor through the CLT and CDM model proposed by Murakami and his colleagues (2012) and Kanagawa et al. (1996). We have also proved that the estimated stiffness agrees with the finite element calculations and experimental results (Talreja, 1985). This approach is extended to a three-dimensional model (Onodera and Okabe, 2019) using a sophisticated model proposed by Li et al. (2019). However, the effective compliance matrix proposed by Murakami and his colleagues (2012) is asymmetric. This asymmetry of the compliance matrix was also observed in the study done by Lee et al. (1989). Furthermore, because the damage tensor is derived by solving the Laplace equation, it is written as a complicated infinite series (Okabe et al., 2018).

The fiber breakage generally causes nonlinearity in the stress–strain curves when the applied strain is large. It is well known that Rosen (1994) originally studied the stress transfer length around fiber breaks as well as the unidirectional composite failure strength and applied to glass-epoxy monolayer specimens. Analytical models considering fiber breakage have been mainly developed in the field of ceramic matrix composites (CMCs) since the late-1980s. This is because a stress concentration due to a fiber break can almost be neglected, so that the global load sharing model (GLS), wherein the load shed by a broken fiber is shared by all intact fibers, can be directly applied to the experiments. Curtin (1991) presents a famous theory to predict the ultimate tensile strength of the unidirectional composites assuming the GLS model. Neumeister (1993) developed an approximate solution of the stress–strain curve and strength of the composite and compared to a numerical result based on the fiber fragmentation theory formulated by Curtin (1991). Hui et al. (1995) derived an explicit closed-form solution of the evolution of fiber fragments and applied to estimate the strength of unidirectional composite materials. In general, the GLS models give a larger strength than the local load-sharing (LLS) model that considers local stress concentrations caused by fiber breaks (Ibnabdeljalil and Curtin, 1997). However, the GLS models are theoretically easy to handle. Therefore, it is suitable to utilize the GLS models to analytically formulate the damage tensor.

This study developed an appropriate expression for the effective stiffness matrix of damaged composite laminates and derived simplified expressions for the damage tensor with the fiber breakage and transverse crack density. Damage variable for fiber breakage was formulated using the GLS model for unidirectional fiber-reinforced composites. An approximate simplified expression for the damage tensor with transverse crack density was obtained from the Laplace equation, assuming the quadratic function. For validating the present model, the obtained damage tensor was substituted into CDM and CLT models, and the elastic constants of damaged composite laminates were then predicted for cross-ply and angle-ply laminates. As for the appropriate expression for the effective compliance/stiffness matrix of a damaged ply, we verified four types of damage matrices including the Murakami (2012) (Kanagawa et al., 1996), Yoshimura (2011), Li et al. (2019) and Maimí models (Maimí et al., 2007). We determined that the Maimí model was the most appropriate among these four models. Moreover, we succeeded in simplifying the expression for damage variables with complicated infinite series obtained in our previous study. We also proved that this could contribute toward the improving the analysis accuracy. Further, we determined the nonlinear stress–strain response and ultimate tensile strength of CFRP and glass-fiber-reinforced-plastic (GFRP) cross-ply

laminates. We employed the Maimí model and simplified damage variables proposed in this study when calculating the stress–strain response. The ultimate tensile strength of CFRP cross-ply laminates was predicted based on a strain-based fiber failure criterion (McCartney, 2005) because fiber fracture in CFRP laminates often occurs at the point of laminate failure. For GFRP laminates, the stiffness reduction due to multiple-fiber fragmentation in  $0^\circ$  plies and the subsequent final laminate failure were determined using the GLS model.

## Model formulation

### Effective elastic compliance/stiffness matrix of damaged ply

Four models for the elastic compliance matrix of a damaged composite ply under the plane stress condition are introduced here, and their characteristics are explained.

#### Model 1: Murakami model

Murakami published a sophisticated book (Murakami, 2012) introducing CDM and proposed a compliance matrix for damaged composite plies with his colleagues (Kanagawa et al., 1996). They used the strain equivalent principle to obtain the following stress–strain relationship

$$\begin{pmatrix} \varepsilon_{11} \\ \varepsilon_{22} \\ 2\varepsilon_{12} \end{pmatrix} = \begin{pmatrix} \frac{1}{(1-d_{11})E_1} & -\frac{\nu_{12}}{(1-d_{22})E_1} & 0 \\ -\frac{\nu_{12}}{(1-d_{11})E_1} & \frac{1}{(1-d_{22})E_2} & 0 \\ 0 & 0 & \frac{1}{2}\left(\frac{1}{1-d_{11}} + \frac{1}{1-d_{22}}\right)\frac{1}{G_{12}} \end{pmatrix} \begin{pmatrix} \sigma_{11} \\ \sigma_{22} \\ \sigma_{12} \end{pmatrix} \quad (1)$$

$E_i$  is the Young's modulus,  $G_{ij}$  is the shear modulus,  $\nu_{ij}$  is the Poisson's ratio,  $\varepsilon_{ij}$  is the strain tensor,  $\sigma_{ij}$  is the stress tensor, and  $d_{ij}$  is the damage variable. In equation (1), subscripts 1 and 2 denote the fiber direction and the in-plane transverse direction, respectively. In our previous study, we found that this matrix is effective for obtaining the elastic constants of damaged composite laminates if the appropriate damage tensor is used. However, the compliance matrix in equation (1) is obviously asymmetric, and this violates the existence of the strain energy function. Moreover, this form cannot be directly entered into the numerical simulation code as in FEA. As stated above, this asymmetry of the compliance matrix was also observed in the work of Lee et al. (1989).

#### Model 2: Yoshimura model

Yoshimura et al. (2011) proposed the concept of the stress equivalent principle to overcome the difficulty of the asymmetry of the compliance matrix. The stress–strain relation can be written as

$$\begin{pmatrix} \sigma_{11} \\ \sigma_{22} \\ \sigma_{12} \end{pmatrix} = \begin{pmatrix} B_{11} & B_{12} & 0 \\ & B_{22} & 0 \\ \text{sym.} & & B_{33} \end{pmatrix} \begin{pmatrix} \varepsilon_{11} \\ \varepsilon_{22} \\ 2\varepsilon_{12} \end{pmatrix} \quad (2)$$

where

$$B_{11} = \frac{(1 - d_{11})E_1}{1 - \nu_{12}\nu_{21}} - \frac{d_{11}^2 \nu_{12}\nu_{21}(1 + \nu_{23})E_1}{4 \Delta(1 - \nu_{12}\nu_{21})} \quad (3)$$

$$B_{12} = \frac{\left(1 - \frac{d_{11} + d_{22}}{2}\right)\nu_{12}E_2}{1 - \nu_{12}\nu_{21}} - \frac{d_{11}d_{22} \nu_{12}(\nu_{23} + \nu_{12}\nu_{21})E_2}{4 \Delta(1 - \nu_{12}\nu_{21})} \quad (4)$$

$$B_{22} = \frac{(1 - d_{22})E_2}{1 - \nu_{12}\nu_{21}} - \frac{d_{22}^2 (\nu_{23} + \nu_{12}\nu_{21})^2 E_2}{4 \Delta(1 + \nu_{23})(1 - \nu_{12}\nu_{21})} \quad (5)$$

$$B_{33} = \left(1 - \frac{d_{11} + d_{22}}{2}\right)G_{12} \quad (6)$$

$$\Delta = 1 - \nu_{23} - 2\nu_{12}\nu_{21} \quad (7)$$

In this case, the stiffness matrix is obviously symmetric. This effective stiffness matrix has already been inserted into the ABAQUS user subroutine to simulate the high-velocity impact problem. The simulation results roughly reproduced the damage progress observed experimentally, but the simulation underestimated the extent of damage compared to the experiments. Moreover, the degradation coefficient of shear modulus does not have any physical meaning. These points are discussed later when comparing the four models explained in this section.

### Model 3: Li model

Li et al. (2019) formulated the three-dimensional effective stiffness matrix for a ply with transverse cracking assuming a small damage. The two-dimensional effective stiffness matrix can be written as

$$\begin{pmatrix} \sigma_{11} \\ \sigma_{22} \\ \sigma_{12} \end{pmatrix} = \begin{pmatrix} C_{11} - \frac{C_{13}^2}{C_{33}} & C_{12} - \frac{C_{13}C_{23}}{C_{33}} & 0 \\ & C_{22} - \frac{C_{23}^2}{C_{33}} & 0 \\ \text{sym.} & & C_{66} \end{pmatrix} \begin{pmatrix} \varepsilon_{11} \\ \varepsilon_{22} \\ 2\varepsilon_{12} \end{pmatrix} \quad (8)$$

where

$$C_{11} = \frac{1 - \nu_{23}}{\Delta} E_1 - \omega \frac{E_1 \nu_{12} \nu_{21}}{\Delta^2} \quad (9)$$

$$C_{12} = \frac{\nu_{12}}{\Delta} E_2 - \omega \frac{E_2 \nu_{12} (1 - \nu_{12} \nu_{21})}{(1 + \nu_{23}) \Delta^2} \quad (10)$$

$$C_{13} = \frac{\nu_{12}}{\Delta} E_2 - \omega \frac{E_2 \nu_{12} (\nu_{23} + \nu_{12} \nu_{21})}{(1 + \nu_{23}) \Delta^2} \quad (11)$$

$$C_{22} = \frac{1 - \nu_{12} \nu_{21}}{(1 + \nu_{23}) \Delta} E_2 - \omega \frac{E_2 (1 - \nu_{12} \nu_{21})^2}{(1 + \nu_{23})^2 \Delta^2} \quad (12)$$

$$C_{23} = \frac{\nu_{23} + \nu_{12} \nu_{21}}{(1 + \nu_{23}) \Delta} E_2 - \omega \frac{E_2 (1 - \nu_{12} \nu_{21}) (\nu_{23} + \nu_{12} \nu_{21})}{(1 + \nu_{23})^2 \Delta^2} \quad (13)$$

$$C_{33} = \frac{1 - \nu_{12} \nu_{21}}{(1 + \nu_{23}) \Delta} E_2 - \omega \frac{E_2 (\nu_{23} + \nu_{12} \nu_{21})^2}{(1 + \nu_{23})^2 \Delta^2} \quad (14)$$

$$C_{66} = G_{12} - \xi \omega G_{12} \quad (15)$$

Here,  $\omega$  is the damage parameter related to tensile damage, and  $\xi$  is the constant damage parameter related to shear damage.  $\omega$  and  $\xi$  can be expressed as follows (Onodera and Okabe, 2019)

$$\omega = 1 - \frac{E_2^d}{E_2} = d_{22} \quad (16)$$

$$\xi = \frac{1}{\omega} \left( 1 - \frac{G_{12}^d}{G_{12}} \right) \approx \frac{1}{\lambda} \quad (17)$$

Here, superscript  $d$  denotes the property of the damaged ply and  $\lambda$  is the material constant described later. Onodera and Okabe (2019) utilized this effective stiffness for predicting the stiffness reduction and steady-state cracking of laminates with ply cracking. The proposed CDM model agrees with the experimental and numerical results (Onodera and Okabe, 2019). However, the damage parameter  $\omega$  and transverse crack density have upper limits because a small damage was assumed.

#### Model 4: Maimí model

Maimí et al. (2007) proposed the complementary free energy function and thermodynamically derived the effective compliance matrix as follows

$$\begin{pmatrix} \varepsilon_{11} \\ \varepsilon_{22} \\ 2\varepsilon_{12} \end{pmatrix} = \begin{pmatrix} \frac{1}{(1-d_{11})E_1} & -\frac{\nu_{12}}{E_1} & 0 \\ & \frac{1}{(1-d_{22})E_2} & 0 \\ \text{sym.} & & \frac{1}{(1-d_{12})G_{12}} \end{pmatrix} \begin{pmatrix} \sigma_{11} \\ \sigma_{22} \\ \sigma_{12} \end{pmatrix} \quad (18)$$

The effective compliance matrix in this case is also explicitly symmetric. However, this case needs an additional damage variable  $d_{12}$  for evaluating the shear stiffness reduction due to transverse cracks or fiber breaks. For the ply with transverse cracks, this parameter is derived from the displacement field of the damaged ply in this study. For the ply with fiber breaks,  $d_{12}$  can be approximated as follows (Murakami, 2012)

$$\frac{1}{1-d_{12}} = \frac{1}{2} \left( \frac{1}{1-d_{11}} + 1 \right) \quad (19)$$

The approximate relation of equation (19) was used when considering the ply with fiber breaks.

### Damage variables

*Damage variable  $d_{11}$  for multi-fiber fragmentation.* An analytical expression for  $d_{11}$  was developed by employing Curtin's GLS model (1991) considering the ultimate tensile strength of unidirectional fiber-reinforced composites. Now, we consider the mechanical equilibrium on an arbitrary cross-section in a unidirectional fiber-reinforced composite with broken fibers. Utilizing the shear-lag model, the slip length  $l_f$  can be described as

$$l_f = \frac{rT}{2\tau} \quad (20)$$

where  $T$  is the far-field axial fiber stress,  $\tau$  is the fiber/matrix interfacial sliding stress, and  $r$  is the fiber radius. If fiber breaks occur equally within the range  $\pm l_f$ , then the average stress carried by the broken fibers in the selected plane is half of that carried by the unbroken fibers. The stress carried by the broken, and unbroken fibers in the selected plane can be described as

$$\bar{\sigma}_f = T \{ 1 - P_f(T, 2l_f) \} + \frac{T}{2} P_f(T, 2l_f) \quad (21)$$

Here, the first term on the right-hand side represents the load carried by the unbroken fiber with the fraction  $1 - P_f(T, 2l_f)$ , and the second term is the average load carried by the broken fibers, whose fraction is  $P_f(T, 2l_f)$ . It is well known that the probability  $P_f(T, 2l_f)$  of the fiber failure with applied stress  $T$  and length  $2l_f$  can be simplified as

$$P_f(T, 2l_f) \approx \frac{2l_f}{L_0} \left( \frac{T}{\sigma_0} \right)^m = \left( \frac{T}{\sigma_c} \right)^{m+1} \quad \text{if} \quad \frac{2l_f}{L_0} \left( \frac{T}{\sigma_0} \right)^m \ll 1 \quad (22)$$

where  $m$  is the Weibull modulus and  $\sigma_0$  is the mean strength at gauge length  $L_0$ .  $\sigma_c$  is the characteristic strength defined as follows

$$\sigma_c = \left( \frac{\sigma_0 \tau L_0}{r} \right)^{1/(m+1)} \quad (23)$$

In the selected cross section, the following mechanical equilibrium condition must be satisfied

$$\sigma_1 = f\bar{\sigma}_f \quad (24)$$

$\sigma_1$  is the stress applied on the unidirectional composite along the fiber direction and  $f$  is the fiber volume fraction. Using the Voigt model for representing the Young's modulus of composite, the unidirectional axial composite stress  $\sigma_1$ , axial fiber stress  $T$ , and unidirectional Young's modulus  $E_1$  are expressed as

$$\sigma_1 = (1 - d_{11})E_1\varepsilon_1 \quad (25)$$

$$T = E_f\varepsilon_1 \quad (26)$$

$$E_1 = fE_f + (1 - f)E_m \approx fE_f \quad (27)$$

Here,  $\varepsilon_1$  is the unidirectional composite strain,  $E_f$  is the fiber axial modulus, and  $E_m$  is the matrix modulus. We neglected the term  $(1 - f)E_m$  in equation (27) because  $E_f \gg E_m$  is approximately satisfied in the case of polymer matrix composites. Using equations (21), (22), and (25) to (27) in equation (24), the damage variable was simply derived as

$$d_{11} = \frac{1}{2} \left( \frac{T}{\sigma_c} \right)^{m+1} \quad (28)$$

The remaining unknown variable is the far-field fiber axial stress  $T$ . Substituting equations (21) and (22) into equation (24), the following nonlinear equation for  $T$  was obtained

$$\sigma_1 = fT \left( 1 - \frac{1}{2} \left( \frac{T}{\sigma_c} \right)^{m+1} \right) \quad (29)$$

Stress  $T$  at applied load  $\sigma_1$  was numerically obtained by solving the above nonlinear equation. When a cross-ply laminate having  $0^\circ$  plies with volume fraction  $V_1$  and the  $90^\circ$  plies with volume fraction  $V_2$  is considered, the applied axial laminate stress  $\bar{\sigma}_L$  can be described using the rule of mixture as follows

$$\bar{\sigma}_L = V_1\sigma_1 + V_2\sigma_2 \approx V_1\sigma_1 \quad (30)$$

$\sigma_1$  is the  $0^\circ$  ply stress and  $\sigma_2$  is the  $90^\circ$  ply stress. We decided to neglect the second term on the right-hand side in equation (30). This is because fiber breaks in the  $0^\circ$  ply may start after the saturation of transverse cracks, and the  $90^\circ$  plies have a very small load-bearing capacity during saturation of transverse cracks. Using equation (30) in equation (29), the nonlinear expression for stress  $T$  is rewritten as

$$\frac{\bar{\sigma}_L}{V_1} = fT \left( 1 - \frac{1}{2} \left( \frac{T}{\sigma_c} \right)^{m+1} \right) \quad (31)$$

The ultimate tensile strength of cross-ply laminates can be derived using equation (31). The ultimate failure condition of composite laminates is described by the following equation

$$\frac{d\bar{\sigma}_L}{dT} = 0 \quad (32)$$

The maximum far-field fiber stress  $T_{\max}$  and ultimate tensile strength  $\bar{\sigma}_L^{\text{ULT}}$  of cross-ply laminates were simply obtained by substituting equations (31) into (32)

$$T_{\max} = \left( \frac{2}{m+2} \right)^{1/(m+1)} \sigma_c \quad (33)$$

$$\bar{\sigma}_L^{\text{ULT}} = V_1 f \sigma_c \left( \frac{2}{m+2} \right)^{1/(m+1)} \frac{m+1}{m+2} \quad (34)$$

The maximum value of damage variable  $d_{11}$  was obtained using equation (33) in equation (28)

$$d_{11}^{\max} = \frac{1}{m+2} \quad (35)$$

$d_{11}$  increased to its maximum value in equation (35) under the ultimate tensile failure condition. In this study, the far-field stress  $T$  was calculated using the Newton method to solve the nonlinear equation (equation (31)) at a given laminate tensile stress  $\bar{\sigma}_L$  until the ultimate tensile failure condition in equation (32) was satisfied.  $d_{11}$  was obtained using the calculated stress  $T$  in equation (28).

**Damage variable  $d_{22}$  associated with transverse cracking.** In any of the effective stiffness/compliance models stated above,  $d_{22}$  is necessary to evaluate the compliance/stiffness matrix of the damaged ply. The governing equation (i.e. Laplace equation) of the corresponding problem was derived. The simplified solution of the equation obtained assuming that the displacement field in the longitudinal direction can be expressed as a quadric function. Further, the boundary condition for the governing equation was loosened.

As shown in Figure 1, the solved problem is the displacement field for the damaged transverse ply including periodic matrix cracks having an interval of  $2l$ . These matrix cracks fully propagate in the  $z$ -direction and reach the interface. The longitudinal strain of the neighboring ply is assumed to be uniform and unaffected by these cracks. Considering the symmetry of the problem, only the first quadrant in the  $xy$  plane was addressed. The plane strain condition was assumed, and the constitutive relations are given by

$$\varepsilon_{xx}(x, y) = \frac{\partial u(x, y)}{\partial x} = C_1 \sigma_{xx}(x, y) - C_2 \sigma_{yy}(x, y) \quad (36)$$

$$\varepsilon_{yy}(x, y) = \frac{\partial v(x, y)}{\partial y} = C_1 \sigma_{yy}(x, y) - C_2 \sigma_{xx}(x, y) \quad (37)$$

$$\gamma_{xy}(x, y) = \frac{\sigma_{xy}(x, y)}{G_{23}} = \frac{\partial v(x, y)}{\partial x} + \frac{\partial u(x, y)}{\partial y} \approx \frac{\partial v(x, y)}{\partial x} \quad (38)$$

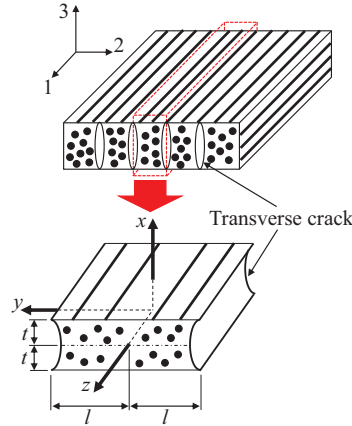


**Figure 1.** Representative volume element in a cracked ply with transverse crack spacing  $2l$  and ply thickness  $2t$ .  $(1, 2, 3)$  is the material coordinate system, and  $(x, y, z)$  is the representative volume element coordinate system.

Here,  $u$  and  $v$  are the displacements along the  $x$  and  $y$  directions, respectively.  $C_1$  and  $C_2$  are given by

$$C_1 = \frac{1 - \nu_{12}\nu_{21}}{E_2}, \quad C_2 = \frac{\nu_{23} + \nu_{12}\nu_{21}}{E_2} \tag{39}$$

We assumed that  $\partial u/\partial y$  was negligible in equation (38) so that the compatible condition of the strain tensor was not satisfied. To obtain the governing equation for displacement  $v$ , the following relationship was introduced

$$\varepsilon_{xx}(x, y) = a\varepsilon_{yy}(x, y) \tag{40}$$

where  $a$  is the effective Poisson's ratio derived from the equilibrium equation. Substituting equation (40) into equations (36) and (37), we obtained the stress with displacement  $v$  as follows

$$\sigma_{xx}(x, y) = \frac{aC_1 + C_2}{C_1^2 - C_2^2} \frac{\partial v(x, y)}{\partial y} \tag{41}$$

$$\sigma_{yy}(x, y) = \frac{C_1 + aC_2}{C_1^2 - C_2^2} \frac{\partial v(x, y)}{\partial y} \tag{42}$$

These stresses satisfy the following two-dimensional equilibrium equations

$$\frac{\partial \sigma_{xx}}{\partial x} + \frac{\partial \sigma_{xy}}{\partial y} = 0 \tag{43}$$

$$\frac{\partial \sigma_{xy}}{\partial x} + \frac{\partial \sigma_{yy}}{\partial y} = 0 \tag{44}$$

Substituting equations (38) and (41) into equation (43) and removing the trivial case (i.e.  $\partial^2 v / \partial x \partial y \neq 0$ ),  $a$  was calculated as

$$\begin{aligned} a &= -\frac{C_2 + G_{23}(C_1^2 - C_2^2)}{C_1} \\ &= -\frac{E_2(\nu_{23} + \nu_{12}\nu_{21}) + G_{23}\{(1 - \nu_{12}\nu_{21})^2 - (\nu_{23} + \nu_{12}\nu_{21})^2\}}{E_2(1 - \nu_{12}\nu_{21})} \end{aligned} \quad (45)$$

Furthermore, substituting equations (38) and (42) into equation (44), the following governing equation of the displacement field was obtained

$$\frac{\partial^2 v}{\partial x^2} + \lambda^2 \frac{\partial^2 v}{\partial y^2} = 0 \quad (46)$$

where

$$\lambda = \sqrt{\frac{C_1 + aC_2}{G_{23}(C_1^2 - C_2^2)}} = \sqrt{\frac{E_2 - G_{23}(\nu_{23} + \nu_{12}\nu_{21})}{G_{23}(1 - \nu_{12}\nu_{21})}} \quad (47)$$

The boundary condition of the governing equation is written as

$$\sigma_{xy}(0, y) = 0 \iff \frac{\partial v}{\partial x}(0, y) = 0 \quad (48)$$

$$v(t, y) = \varepsilon_{yy}^\infty \quad (49)$$

$$v(x, 0) = 0 \quad (50)$$

$$\sigma_{yy}(x, l) = 0 \iff \frac{\partial v}{\partial y}(x, l) = 0 \quad (51)$$

where  $\varepsilon_{yy}^\infty$  is the applied strain of the ply parallel to the  $y$ -axis and  $2t$  is the ply thickness. The displacement field can be solved with equation (46). In our previous study (Okabe et al., 2018), this partial differential equation was solved by the variable separation method. However, the obtained solution was an infinite series and very complicated. Therefore, this study obtained a simplified form of the displacement field.

To obtain the simplified solution, the displacement form of the following type was assumed

$$v(x, y) = A(y)x^2 + B(y)x + C(y) \quad (52)$$

Using the displacement in equation (52) in equations (48) and (49) yielded

$$B(y) = 0 \quad (53)$$

$$C(y) = \varepsilon_{yy}^{\infty} y - A(y)t^2 \quad (54)$$

Thus, equation (52) can be written as

$$v(x, y) = A(y)(x^2 - t^2) + \varepsilon_{yy}^{\infty} y \quad (55)$$

Next, our main task was to explicitly determine  $A(y)$ . The boundary condition of equation (50) gives

$$A(0) = 0 \quad (56)$$

However, it is impossible to satisfy the boundary condition of equation (51) exactly as it is. Thus, according to McCartney (1992), the following averaged boundary condition was used

$$\frac{1}{t} \int_0^t \frac{\partial v(x, l)}{\partial y} dx = 0 \quad (57)$$

Hence, using equation (55) into equation (57) results in

$$\frac{dA(l)}{dy} = \frac{3\varepsilon_{yy}^{\infty}}{2t^2} \quad (58)$$

Similar to equation (51), the government equation, i.e. equation (46), cannot be solved directly. Instead of equation (46), the following averaged government equation was here solved

$$\frac{1}{t} \int_0^t \left( \frac{\partial^2 v}{\partial x^2} + \lambda^2 \frac{\partial^2 v}{\partial y^2} \right) dx = 0 \quad (59)$$

Using equation (55) in equation (59) yielded the following ordinary differential equation

$$\frac{d^2 A(y)}{dy^2} - \beta^2 A(y) = 0 \quad (60)$$

where

$$\beta = \frac{\sqrt{3}}{\lambda t} \quad (61)$$

The solution of equation (60) with the boundary conditions in equations (56) and (58) is

$$A(y) = \frac{3\varepsilon_{yy}^{\infty} \sinh \beta y}{2t^2 \beta \cosh \beta l} \quad (62)$$

Thus, it can be shown that

$$v(x, y) = \frac{3\varepsilon_{yy}^{\infty} \sinh\beta y}{2t^2\beta \cosh\beta l} (x^2 - t^2) + \varepsilon_{yy}^{\infty} y \quad (63)$$

As stated in our previous paper (Okabe et al., 2018), the damage variable is the ratio of the inelastic strain due to crack opening to the total strain and is finally given by

$$d_{22} = \frac{\varepsilon_{yy}^{\infty} - \frac{1}{l} \int_0^l v(x, l) dx}{\varepsilon_{yy}^{\infty}} = \frac{\tanh\beta l}{\beta l} = \frac{2\rho}{\beta} \tanh \frac{\beta}{2\rho} \quad (64)$$

where  $\rho = 1/(2l)$  is the transverse crack density in the damaged ply. As stated above, we derived the following equation (Okabe et al., 2018)

$$d_{22} = 1 - \frac{8}{\pi^3 \lambda t} \sum_{n=1}^{\infty} \frac{1}{(2n-1)^3} \frac{\tanh[(2n-1)\pi\lambda t\rho]}{\rho} \quad (65)$$

Equation (64) is obviously simpler than equation (65), and loosening the boundary condition equation (51) increases crack opening so that equation (64) gives better predictions than equation (65) in some cases. We will describe this section later through verifications and validations.

**Damage variable  $d_{12}$  associated with transverse cracking.** When the effective compliance matrix shown in equation (18) is used, the analytical form for damage variable  $d_{12}$  is required. The schematic shown in Figure 1 is also considered here. The neighboring ply deforms under a constant shear strain  $\gamma_{yz}^{\infty}$  in the  $yz$  plane, and the displacement field is assumed as

$$u(x, y, z) = v(x, y, z) = 0 \quad (66)$$

$$w = w(x, y) \quad (67)$$

Thus, these equations give  $\sigma_x = \sigma_y = \sigma_z = \sigma_{xy} = 0$  and  $\varepsilon_x = \varepsilon_y = \varepsilon_z = \gamma_{xy} = 0$  so that the out of plane shear stresses are nonzero and given as

$$\sigma_{xz}(x, y) = G_{12}\gamma_{xz}(x, y) = G_{12} \frac{\partial w(x, y)}{\partial x} \quad (68)$$

$$\sigma_{yz}(x, y) = G_{12}\gamma_{yz}(x, y) = G_{12} \frac{\partial w(x, y)}{\partial y} \quad (69)$$

The stresses should satisfy the following three-dimensional equilibrium equations

$$\frac{\partial \sigma_{xx}}{\partial x} + \frac{\partial \sigma_{xy}}{\partial y} + \frac{\partial \sigma_{xz}}{\partial z} = 0 \quad (70)$$

$$\frac{\partial \sigma_{xy}}{\partial x} + \frac{\partial \sigma_{yy}}{\partial y} + \frac{\partial \sigma_{yz}}{\partial z} = 0 \quad (71)$$

$$\frac{\partial \sigma_{xz}}{\partial x} + \frac{\partial \sigma_{yz}}{\partial y} + \frac{\partial \sigma_{zz}}{\partial z} = 0 \quad (72)$$

These stresses given in equations (68) and (69) automatically satisfy equations (70) and (71) and lead to the following governing equation derived from equation (72)

$$\frac{\partial^2 w}{\partial x^2} + \frac{\partial^2 w}{\partial y^2} = 0 \quad (73)$$

As mentioned in the previous section, the following boundary conditions should be satisfied:

$$\sigma_{xz}(0, y) = 0 \iff \frac{\partial w}{\partial x}(0, y) = 0 \quad (74)$$

$$w(t, y) = \gamma_{yz}^\infty y \quad (75)$$

$$w(x, 0) = 0 \quad (76)$$

$$\sigma_{yz}(x, l) = 0 \iff \frac{\partial w}{\partial y}(x, l) = 0 \quad (77)$$

This boundary problem defined by equations (73) to (77) is almost the same as the one defined by equations (46) to (51); therefore, the same derivation procedure can be adopted for this boundary problem. Thus, the displacement field is given by

$$w(x, y) = \frac{3\gamma_{yz}^\infty}{2t^2\beta_{12}} \frac{\sinh\beta_{12}y}{\cosh\beta_{12}l} (x^2 - t^2) + \gamma_{yz}^\infty y \quad (78)$$

$$\beta_{12} = \frac{\sqrt{3}}{t} \quad (79)$$

The shear damage variable  $d_{12}$  can be defined as

$$d_{12} = 1 - \frac{G_{12}^d}{G_{12}} \quad (80)$$

where  $G_{12}^d$  is the shear stiffness of the ply with transverse cracking. The average ply shear strain  $\gamma_{yz}^{\text{ave}}$  not considering the crack-opening displacement and applied shear strain  $\gamma_{yz}^\infty$  are described as follows

$$\gamma_{yz}^{\text{ave}} = 1 - \frac{\sigma_{yz}}{G_{12}} \quad (81)$$

$$\gamma_{yz}^{\infty} = 1 - \frac{\sigma_{yz}}{G_{12}^d} \quad (82)$$

Substituting equations (81) and (82) into equation (80),  $d_{12}$  can be rewritten as

$$d_{12} = 1 - \frac{\gamma_{yz}^{\text{ave}}}{\gamma_{yz}^{\infty}} \quad (83)$$

The average shear strain is defined by

$$\gamma_{yz}^{\text{ave}} = \frac{1}{lt} \int_0^l w(x, l) dx \quad (84)$$

We obtained  $d_{12}$  from equations (78), (83), and (84)

$$d_{12} = \frac{\gamma_{yz}^{\infty} - \frac{1}{lt} \int_0^l w(x, l) dx}{\gamma_{yz}^{\infty}} = \frac{\tanh \beta_{12} l}{\beta_{12} l} = \frac{2\rho}{\beta_{12}} \tanh \frac{\beta_{12}}{2\rho} \quad (85)$$

The reduction in shear modulus was initially determined by Hashin (1986), by using the variation approach. Recently, Onodera and Okabe (2019) also obtained the shear damage variable with an infinite series

$$d_{12} = 1 - \frac{8}{\pi^3 t} \sum_{n=1}^{\infty} \frac{1}{(2n-1)^3} \frac{\tanh[(2n-1)\pi t \rho]}{\rho} \quad (86)$$

However, equation (85) is obviously simpler than the infinite series of equation (86).

### *Effective elastic constants for the damaged composite laminates*

The substitution of damage variables  $d_{22}$  and  $d_{12}$  into equations (1), (2), (8), and (18) gives the effective compliance/stiffness matrix of a ply with transverse cracks as a function of crack density  $\rho$ , and fiber breaks can be considered by substituting  $d_{11}$  into equations (1), (2), and (18). The effective stiffness of composite laminates with transverse cracks can be estimated through the CLT using the effective compliance matrix of a damaged ply.

Let us consider the coordinate systems shown in Figure 2. The effective compliance matrix and thermal expansion coefficient of the  $k$ th ply having transverse crack density  $\rho$  in material coordinate system (1, 2, 3) are defined as  $\mathbf{C}_k(\rho)$  and  $\boldsymbol{\alpha}_k$ , respectively. Similarly, those of laminate coordinate system (X, Y, Z) are defined as  $\bar{\mathbf{C}}_k(\rho)$  and  $\bar{\boldsymbol{\alpha}}_k$ , respectively. When the fiber angle is given by  $\theta_k$ ,  $\bar{\mathbf{C}}_k(\rho)$  and  $\bar{\boldsymbol{\alpha}}_k$  are given as

$$\bar{\mathbf{C}}_k(\rho) = \mathbf{R}_k \mathbf{C}_k(\rho) \mathbf{T}_k^{-1} \quad (87)$$

$$\bar{\boldsymbol{\alpha}}_k = \mathbf{R}_k \boldsymbol{\alpha}_k \quad (88)$$

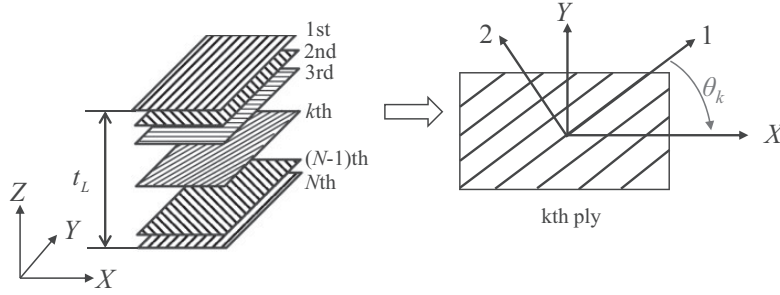


**Figure 2.** Relationship between the laminate coordinate system ( $X, Y, Z$ ) and material coordinate system (1, 2, 3).

where

$$\alpha_k = [\alpha_{11} \quad \alpha_{22} \quad 0]^T \quad (89)$$

$$\mathbf{R}_k = \begin{bmatrix} \cos^2\theta_k & \sin^2\theta_k & -\sin\theta_k\cos\theta_k \\ \sin^2\theta_k & \cos^2\theta_k & \sin\theta_k\cos\theta_k \\ 2\sin\theta_k\cos\theta_k & -2\sin\theta_k\cos\theta_k & \cos^2\theta_k - \sin^2\theta_k \end{bmatrix} \quad (90)$$

$$\mathbf{T}_k = \begin{bmatrix} \cos^2\theta_k & \sin^2\theta_k & -2\sin\theta_k\cos\theta_k \\ \sin^2\theta_k & \cos^2\theta_k & 2\sin\theta_k\cos\theta_k \\ \sin\theta_k\cos\theta_k & -\sin\theta_k\cos\theta_k & \cos^2\theta_k - \sin^2\theta_k \end{bmatrix} \quad (91)$$

where  $\alpha$  is the thermal expansion coefficient. Therefore, according to the CLT, the effective laminate strain  $\bar{\epsilon}_L$  is expressed as

$$\bar{\epsilon}_L = \bar{\mathbf{C}}_L \bar{\sigma}_L + \bar{\alpha}_L \Delta T \quad (92)$$

where the effective stiffness matrix  $\bar{\mathbf{C}}_L(\rho)$  and thermal expansion coefficient  $\bar{\alpha}_L(\rho)$  of the cracked laminate can be written as

$$\bar{\mathbf{C}}_L(\rho) = [\bar{C}_{Lij}] = \left[ \frac{1}{t_L} \sum_{k=1}^N t_k \bar{\mathbf{C}}_k^{-1}(\rho) \right]^{-1} \quad (93)$$

$$\bar{\alpha}_L(\rho) = [\bar{\alpha}_{Li}] = \bar{\mathbf{C}}_L \left[ \frac{1}{t_L} \sum_{k=1}^N t_k \bar{\mathbf{C}}_k^{-1}(\rho) \bar{\alpha}_k \right] \quad (94)$$

$\bar{\sigma}_L$  is the applied axial laminate stress,  $t_L$  is the thickness of the corresponding composite laminates, and  $\Delta T (= T - T_{sf})$  is the difference between the testing temperature  $T$  and stress-free

temperature  $T_{sf}$ . Therefore, the effective elastic constants and effective thermal expansion coefficients of the laminates are given as

$$E_X = \frac{1}{\bar{C}_{11}(\rho)}, \quad E_Y = \frac{1}{\bar{C}_{22}(\rho)}, \quad \nu_{XY} = -\frac{\bar{C}_{12}(\rho)}{\bar{C}_{11}(\rho)}, \quad G_{XY} = \frac{1}{\bar{C}_{66}(\rho)} \quad (95)$$

$$\alpha_X = \bar{\alpha}_{L1}(\rho), \quad \alpha_Y = \bar{\alpha}_{L2}(\rho) \quad (96)$$

We can derive the effective elastic constants analytically with the crack density and fiber breaks through the CLT. The stress-strain relationship of damaged laminates can be obtained using equation (92).

## Results and discussion

### Verification of damage models

The stiffness reduction in laminates with transverse cracking was studied using five approaches for verifying the effective compliance/stiffness matrices and proposed damage variables  $d_{22}$  and  $d_{12}$ . Murakami\_simplified shows the Murakami model using  $d_{22}$  expressed in a simplified form in equation (64). Yoshimura\_simplified is the Yoshimura model with  $d_{22}$  expressed in a simplified form, identical to Murakami\_simplified. Li\_simplified is the Li model including the damage parameter  $\omega$  in equations (16) and (64) and constant damage parameter  $\xi$  in equations (17) and (47). Maimí\_simplified gives the Maimí model with simplified forms of  $d_{22}$  in equation (64) and  $d_{12}$  in equation (85). Maimí\_infinite\_series describes the result of the Maimí model with infinite forms of  $d_{22}$  in equation (65) and  $d_{12}$  in equation (86). In Li\_simplified, the upper limit of the transverse crack density resulting from the assumption of a small damage postulated in Li's effective stiffness matrix was determined in the same manner as in our previous study (Li et al., 2019). Table 1 presents the upper limit of the transverse crack density in GFRP laminates used in Li\_simplified.

For verification, comparisons to results obtained using FEA are presented for  $[90/0]_s$  GFRP cross-ply laminates. The material properties listed in Table 2 were used. Transverse cracks are assumed to exist in the  $90^\circ$  plies and face the outer surface. Gudmundson and Zang (1993) calculated the reduction in Poisson's ratio and Young's modulus due to the increase in the transverse crack density. When the matrix crack faces the surface, the crack length should be doubled to include the surficial effect and satisfy the boundary condition. Therefore, we obtain

$$d_{22} = \frac{4\rho}{\beta} \tanh \frac{\beta}{4\rho} \quad (97)$$

$$d_{12} = \frac{4\rho}{\beta_{12}} \tanh \frac{\beta_{12}}{4\rho} \quad (98)$$

$$d_{22} = 1 - \frac{4}{\pi^3 \lambda t} \sum_{n=1}^{\infty} \frac{1}{(2n-1)^3} \frac{\tanh[2(2n-1)\pi \lambda t \rho]}{\rho} \quad (99)$$

**Table 1.** Upper limit of transverse crack density used in Li\_simplified.

Laminate	Upper limit of transverse crack density (cracks/mm)
GFRP [90/0] <sub>s</sub>	2.01
GFRP [55/−55] <sub>N</sub>	4.02

**Table 2.** Material constants and thickness of GFRP ply used in stiffness reduction calculation Gudmundson and Zhang (1993).

$E_1$ (GPa)	$E_2$ (GPa)	$\nu_{12}$	$\nu_{23}$	$G_{12}$ (GPa)	$G_{23}$ (GPa)	$\alpha_1$ (°C)	$\alpha_2$ (°C)	Ply thickness (mm)
41.7	13	0.3	0.42	3.4	4.58	$6.72 \times 10^{-6}$	$29.3 \times 10^{-6}$	0.203

$$d_{12} = 1 - \frac{4}{\pi^3 t} \sum_{n=1}^{\infty} \frac{1}{(2n-1)^3} \frac{\tanh[2(2n-1)\pi t \rho]}{\rho} \quad (100)$$

The comparison results are shown in Figures 3 and 4. As for Young's modulus, all approaches reproduce the tendency of the results observed in FEA. When comparing Maimí\_simplified and Maimí\_infinite\_series, it is shown that the simple forms of equations (64) and (85) yielded results closer to the FEA results than the infinite series forms of equations (65) and (86). Thus, equations (65) and (86) gave smaller crack openings than the FEA results, and loosening the boundary condition may improve the tendency of the crack opening displacement to match with those obtained using FEA. Murakami\_simplified, Li\_simplified, Maimí\_simplified, and Maimí\_infinite\_series captured the degradation tendency of the Poisson's ratio; however, Yoshimura\_simplified obviously underestimated the degradation. This causes the significant errors in the case of angle-ply laminates because the non-diagonal component directly affects the Young's modulus of the laminate.

Gudmundson and Zhang (1993) also calculated the stiffness reduction in several types of angle-ply laminates using FEA. The present model was verified by comparison with the results for  $[\pm 55]_N$  angle-ply GFRP laminates. The material properties listed in Table 2 were used. Figures 5 to 10 show the changes in the Young's moduli, shear modulus, Poisson's ratio, and thermal expansion coefficients of  $[\pm 55]_N$  laminate as a function of the transverse crack density. Clearly, Maimí\_simplified shows the best agreement among these five approaches for any of the elastic constants, whereas Yoshimura\_simplified cannot capture the trends of Young's modulus and Poisson's ratio at all. As stated above, Poisson's ratio is a critical parameter for evaluating the properties of angle-ply laminates as it reflects the behavior of non-diagonal components in compliance/stiffness matrix. The trends of Yoshimura\_simplified are substantially different from those observed in FEA. Therefore, we do not recommend using Yoshimura\_simplified for evaluating angle-ply laminates.

Although the results obtained using all the models agree well with the FEA results, Maimí\_simplified shows the best agreement. In fact, we proved that Maimí\_simplified is the most appropriate approach among five approaches considering in this study.

### *Nonlinear stress–strain response of CFRP cross-ply laminates*

The nonlinear stress–strain response of CFRP cross-ply laminates resulting from transverse cracking was calculated using the present model and compared to the experimental results obtained in this study. We also applied our model to the results reported by Fikry et al. (2018). The stress–strain

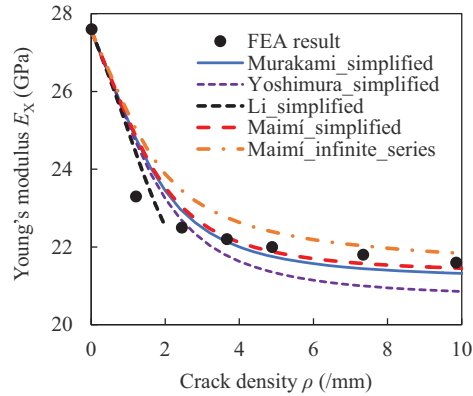


**Figure 3.** Comparison of Young's modulus reduction in GFRP  $[90/0]_s$  laminate due to transverse crack predicted using present models and FEA (Gudmundson and Zhang (1993)).

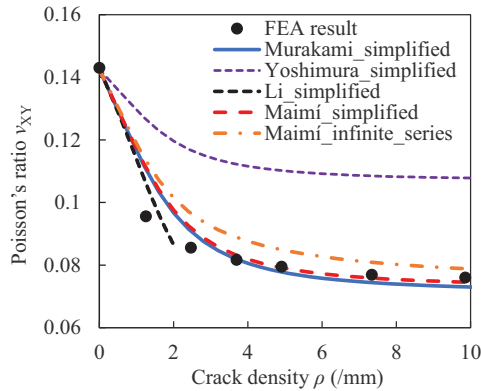


**Figure 4.** Comparison of Poisson's ratio reduction in GFRP  $[90/0]_s$  due to transverse cracking predicted using present models and FEA (Gudmundson and Zhang (1993)).

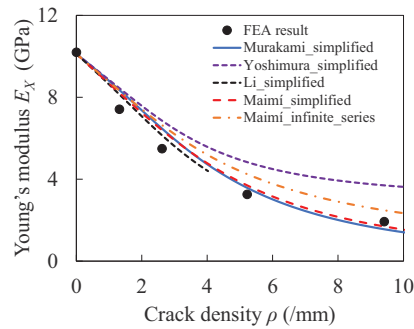


**Figure 5.** Comparison of Young's moduli of GFRP  $[\pm 55]_N$  axial laminates due to transverse cracking predicted by present models and FEA (Gudmundson and Zhang (1993)).

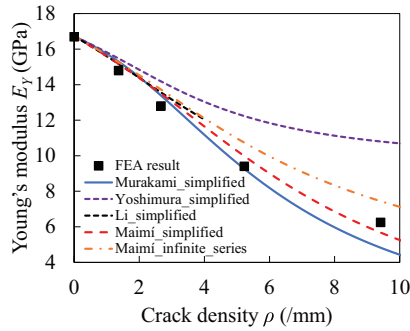


**Figure 6.** Comparison of Young’s moduli reduction in GFRP  $[\pm 55]_N$  transverse laminate due to transverse cracking predicted by present models and FEA (Gudmundson and Zhang (1993)).

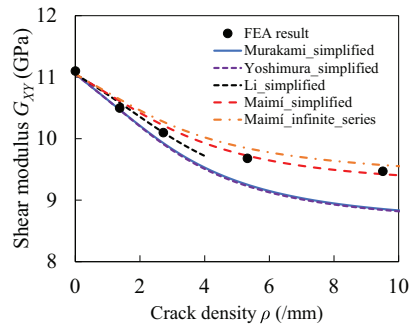


**Figure 7.** Comparison of shear modulus reduction in GFRP  $[\pm 55]_N$  laminate due to transverse cracking predicted by present models and FEA (Gudmundson and Zhang (1993)).

response of cross-ply laminates with transverse cracking was calculated using equations (92) to (94). From the verification result described in the previous section, the effective stiffness model of Maimi\_simplified composed of the Maimi model with simplified forms of  $d_{22}$  in equation (64) and  $d_{12}$  in equation (85) was utilized to predict the stiffness reduction due to transverse cracks in  $90^\circ$  plies. In CFRP laminates subjected to quasi-static monotonic tensile loading, fiber fracture often occurs at the ultimate failure stress of the laminate. Therefore, the stiffness reduction owing to fiber breaks was not considered here, and the ultimate tensile strength of CFRP cross-ply laminates was predicted based on a strain-based fiber failure criterion presented by McCartney (2005) to determine the fracture point in the nonlinear stress–strain curve. In this criterion, the calculated effective laminate axial strain using equation (92) is considered equal to the fiber axial strain in  $0^\circ$  plies. When the effective laminate axial strain is equal to the critical strain,  $\epsilon_{fc}$ , during ultimate fiber failure, ultimate failure of the laminate occurs. The ultimate fiber failure strain,  $\epsilon_{fc}$ , is derived from the spring element model (SEM) simulation (Okabe et al., 2005), which considers the surficial stress concentration obtained from multiple-fiber fragmentation tests (Yamamoto et al., 2019). The bimodal Weibull distribution was applied to reproduce the statistically distributed strength in fibers. A stress concentration factor of 1.9 was used.

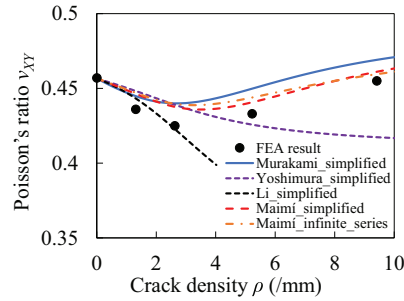


**Figure 8.** Comparison of Poisson's ratio change in GFRP  $[\pm 55]_N$  laminate due to transverse cracking predicted by present models and FEA (Gudmundson and Zhang (1993)).

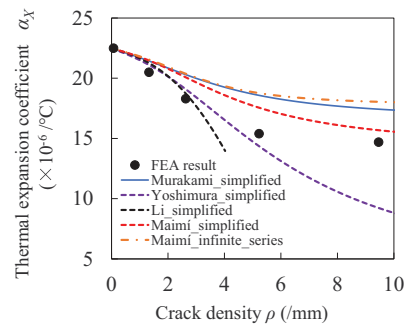


**Figure 9.** Comparison of axial laminate thermal expansion coefficient reduction in GFRP  $[\pm 55]_N$  due to transverse cracking predicted by present models and FEA (Gudmundson and Zhang (1993)).

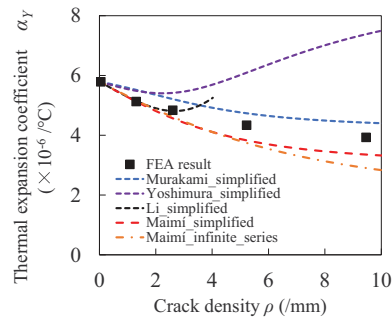


**Figure 10.** Comparison of transverse laminate thermal expansion coefficient reduction in GFRP  $[\pm 55]_N$  due to transverse cracking predicted by present models and FEA (Gudmundson and Zhang (1993)).

The average ultimate fiber failure strain obtained by 100 SEM simulations scaled with each specimen size was regarded as the ultimate fiber failure strain  $\epsilon_{fc}$ . Table 3 lists the material properties of the T700S and resin, and Table 4 shows the bimodal Weibull parameters of the T700S fiber used in SEM simulations. The evolution of transverse crack density  $\rho$  as a function of the applied laminate stress is needed to predict the nonlinear stress–strain curves of the laminates. In this study, to

**Table 3.** Properties of T700S fiber and resin used in SEM simulations (Okabe et al., 2015).

Fiber axial Young's modulus $E_f$ (GPa)	230
Fiber radius $r$ ( $\mu\text{m}$ )	3.5
Matrix Young's modulus $E_m$ (GPa)	3.4
Matrix Poisson's ratio $\nu_m$ (-)	0.31

**Table 4.** Bimodal Weibull parameters of the T700S fiber used in SEM simulations ( Yamamoto et al., 2019).

$\sigma_{01}$ (GPa)	$m_1$	$\sigma_{02}$ (GPa)	$m_2$
5.2	4.8	6.1	12.0

validate the proposed stiffness reduction model, we assumed the following Weibull form for transverse crack density evolution

$$\rho = \rho_s \left[ 1 - \exp \left\{ - \left( \frac{\bar{\sigma}_L - \sigma_{L0}}{\sigma_{Lc}} \right)^{m_T} \right\} \right] \quad (101)$$

where  $\rho_s$  is the saturated transverse crack density,  $\sigma_{L0}$  is the initiation stress of the transverse crack,  $\sigma_{Lc}$  is the Weibull scale parameter, and  $m_T$  is the Weibull modulus. These parameters were determined by fitting with the experimental results.

We performed the experiments by ourselves to validate our model presented in this study. Here, we briefly explain the experimental procedures followed to determine the stiffness reduction, transverse crack density, and stress–strain curves of the cross-ply laminates. Loading and unloading tests were conducted to obtain the nonlinear stress–strain response of cross-ply laminates, transverse crack density in  $90^\circ$  plies, and stiffness reduction. The  $[0/90_8/0]$  cross-ply laminate was composed of T700S/2592 (Toray Industries) unidirectional plies. The laminate specimen had a length, width, and thickness of 249, 25, and 1.42 mm, respectively. A strain gauge (Kyowa Electronic Instruments Co.) was used to measure the strain in the laminate. The free edge of the laminate was polished by a diamond grinding disk (Buehler Ltd.) to observe the transverse crack density. Loading and unloading tests were performed using a servo-hydraulic testing machine MTS810 (MTS Systems Corporation) and involved the following steps: (1) the specimen was loaded with a crosshead speed 1.0 mm/min; (2) when the load reached a specific value, the specimen was held at this load and the transverse cracks were observed at the free edge of the specimen using RepliSet (Struers); (3) the specimen was then unloaded with a crosshead speed 1.0 mm/min until the load reached zero. This loading/unloading cycle comprising steps (1) to (3) was repeated until the specimen failed.

The stress–strain relationship for the T700S/2592  $[0/90_8/0]$  laminate predicted from the present model was compared to the obtained experiment results. We denote T700S/2592 as CFRP-I. The material properties of the ply, parameters of transverse crack evolution, and ultimate fiber failure strain,  $\varepsilon_{fc}$ , derived from SEM simulations are listed in Tables 5 to 7, respectively. The out-of-plane shear modulus,  $G_{23}$ , of CFRP-I ply given in Table 5 was derived as follows

$$G_{23} = \frac{E_2}{2(1 + \nu_{23})} \quad (102)$$

**Table 5.** Mechanical properties of plies used in the calculation of stress-strain behavior of cross-ply laminates.

	CFRP-I (Kumagai et al., 2020)	CFRP-II (Fikry et al., 2018)
Longitudinal Young's modulus $E_1$ (GPa)	115	123
Transverse Young's modulus $E_2$ (GPa)	7.74	8.68
In-plane Poisson's ratio $\nu_{12}$ (-)	0.315	0.33
Out-of-plane Poisson's ratio $\nu_{23}$ (-)	0.394	0.394 <sup>c</sup>
In-plane shear modulus $G_{12}$ (GPa)	3.54	3.92
Out-of-plane shear modulus $G_{23}$ (GPa)	3.78 <sup>a</sup>	2.91 <sup>a</sup>
Longitudinal thermal expansion coefficient $\alpha_1$ ( $10^{-6}/^\circ\text{C}$ )	0.4 <sup>b</sup>	0.4 <sup>b</sup>
Transverse thermal expansion coefficient $\alpha_2$ ( $10^{-6}/^\circ\text{C}$ )	36 <sup>b</sup>	36 <sup>b</sup>
Temperature difference $\Delta T$ ( $^\circ\text{C}$ )	-100	-110
Fiber volume fraction $f$ (-)	0.51	0.528 <sup>d</sup>
Ply thickness (mm)	0.142	0.15

<sup>a</sup> $G_{23}$  was estimated using equation (102).

<sup>b</sup>These values are quoted from Okabe et al. (2015).

<sup>c</sup>This value is quoted from Kumagai et al. (Kumagai et al., 2020).

<sup>d</sup>This was estimated from equation (103).  $E_f$  and  $E_m$  given in Table 3 were used.

**Table 6.** Simulation results of ultimate fiber failure strain at stress concentration factor of 1.9.

	CFRP-I	CFRP-II
Ultimate fiber failure strain $\varepsilon_{fc}$ (%)	1.77	1.83

**Table 7.** Parameters of transverse crack evolution in CFRP laminate used in equation (102).

	CFRP-I	CFRP-II
$\sigma_{L0}$ (MPa)	180	180
$\sigma_{Lc}$ (MPa)	74	110
$m_T$	1.5	1.7
$\rho_s$ (mm)	0.76	0.9

Parameters of transverse crack density evolution were determined by fitting the calculated results of the present model with the experimental data as shown in Figure 11(a). Figure 11(b) presents a comparison of the predicted results for stiffness reduction as a function of transverse crack density determined by using the present model with experimental results. The results predicted using the present model agree quantitatively with the experimental results obtained through loading/unloading tests. The predicted stress-strain responses of the T700S/2592 [0/90<sub>8</sub>/0] laminate were compared to the experimental results, as shown in Figure 11(c). The results of the present model obtained considering stiffness reduction due to transverse cracking show good agreement with the experimental data. According to these results, the nonlinearity of the stress-strain responses observed in the 200–350 MPa range is mainly due to transverse cracking. The ultimate failure stress and strain determined from the critical-strain-based criterion also agree with the experimental data.

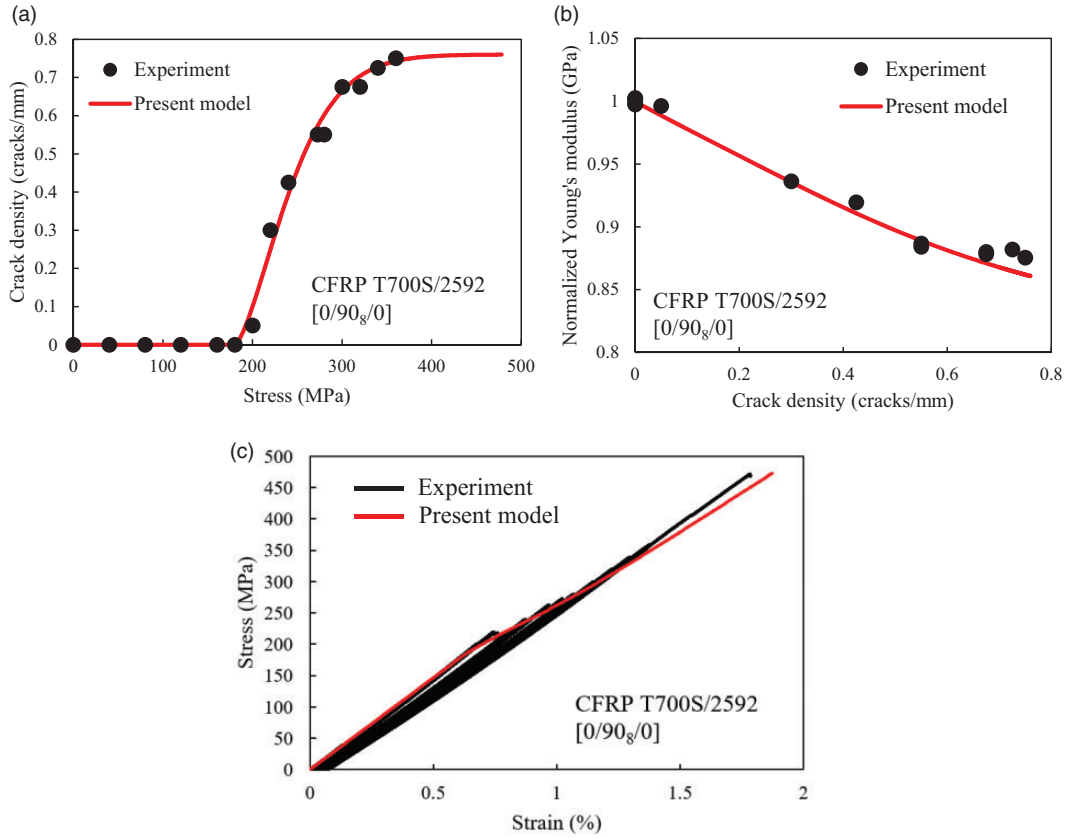


**Figure 11.** Comparison of results predicted using present model for (a) transverse crack density evolution, (b) stiffness reduction, and (c) stress–strain response of T700S/2592 [0/90<sub>8</sub>/0] laminate with experimental results.

This result implies that the ultimate failure strength of CFRP laminates with 0° plies can be determined using the strain-based fiber criterion, and the ultimate fiber failure strain used in this criterion can be predicted through SEM simulations.

The nonlinear stress–strain behavior of the T700SC/2592 [0/90<sub>8</sub>/0] laminate was predicted using the present model, and the results were compared to the experimental result obtained by Fikry et al. (2018). We denote T700SC/2592 as CFRP-II. The material properties of the ply, parameters of transverse crack evolution, and ultimate fiber failure strain,  $\epsilon_{fc}$ , derived from SEM simulations are also listed in Tables 5 to 7, respectively. The out-of-plane shear modulus  $G_{23}$  of CFRP-II ply given in Table 5 was estimated using equation (102). The fiber volume fraction,  $f$ , of CFRP-II is estimated as

$$f = \frac{E_1 - E_m}{E_f - E_m} \tag{103}$$

where  $E_f$  is the fiber axial Young’s modulus and  $E_m$  is the matrix Young’s modulus given in Table 3. The crack evolution parameters used in equation (101) were derived by fitting the predicted results

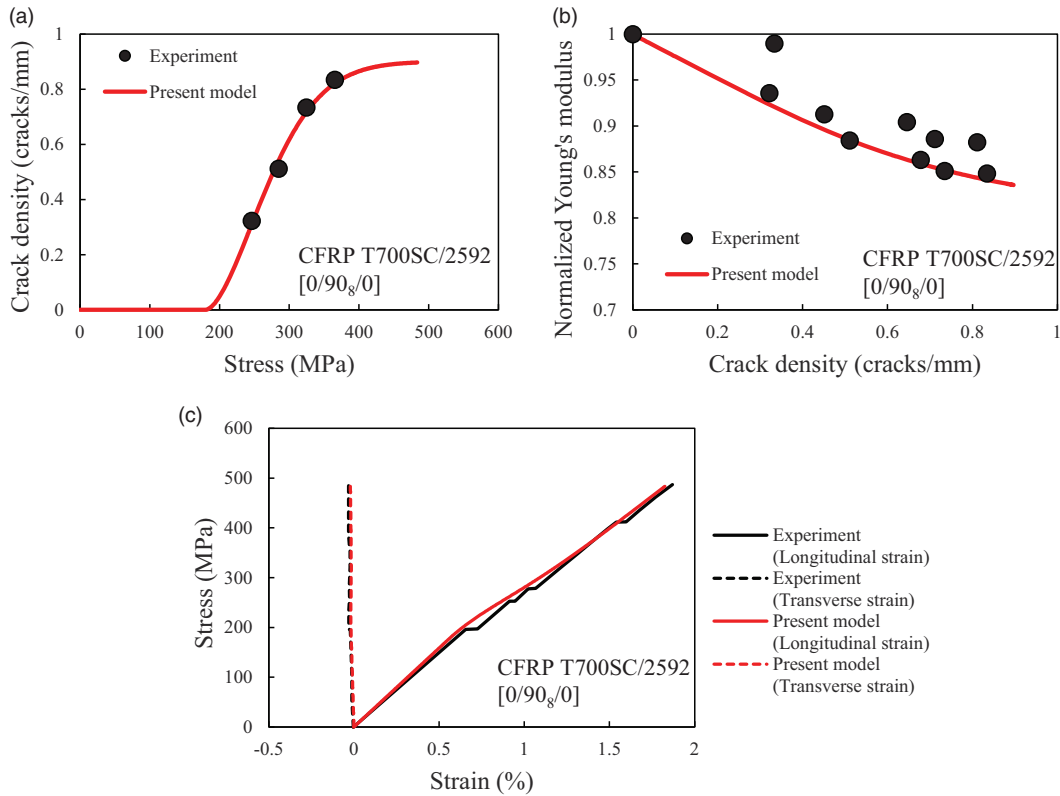


**Figure 12.** Comparison of (a) transverse crack density, (b) stiffness reduction, and (c) stress-strain response of T700SC/2592 [0/90<sub>8</sub>/0] predicted using the present model with experimental results (Fikry et al. (2018)).

with the experiment results, as shown in Figure 12(a). The predicted results for stiffness reduction as a function of the transverse crack density show excellent agreement with the experimental results, as shown in Figure 12(b). Figure 12(c) presents the nonlinear stress as a function of the longitudinal or transverse strain obtained using the present model and through experiments. The present model considering the stiffness reduction due to transverse cracks can predict the nonlinearity of the stress–strain response up to the ultimate failure strength of the laminate estimated using the critical-strain-based criterion.

### Nonlinear stress–strain response of GFRP cross-ply laminates

The nonlinear stress–strain behavior of E-glass/TX24235 GFRP [0/90<sub>n</sub>/0]<sub>s</sub> ( $n = 2, 4, 6$ ) laminates was predicted to validate our proposed damage variables  $d_{11}$ ,  $d_{22}$ , and  $d_{12}$ . The stress–strain responses of cross-ply laminates with transverse cracking and fiber breaks were calculated using equations (92) to (94). The effective stiffness model Maimí\_simplified comprising of the Maimí model with simplified forms of  $d_{22}$  in equation (64) and  $d_{12}$  in equation (85) was utilized to predict the stiffness reduction due to transverse cracks in 90° plies. In the case of GFRP laminates, the stiffness reduction due to multiple-fiber fragmentation in 0° plies and subsequent final laminate failure was calculated using damage variable  $d_{11}$  in equation (28).

The GFRP ply properties were estimated using the analytical model developed by Kravchenko et al. (2017). According to them, the properties of unidirectional-fiber-reinforced ply composed of the transversely isotropic fibers and the isotropic matrix are determined as follows

$$E_1 = E_1^{(f)} f^{(f)} + E^{(m)} f^{(m)} + \left[ \frac{4(\nu^{(m)} - \nu_{12}^{(f)})^2 k^{(m)} k^{(f)} G^{(m)}}{(k^{(f)} + G^{(m)})k^{(m)} + (k^{(f)} - k^{(m)})G^{(m)}f^{(f)}} \right] f^{(f)} f^{(m)} \quad (104)$$

$$E_2 = \left[ \frac{1}{4k_2} + \frac{1}{4G_{23}} + \frac{\nu_{12}^2}{E_1} \right]^{-1} \quad (105)$$

$$\nu_{12} = \nu_{12}^{(f)} f^{(f)} + \nu^{(m)} f^{(m)} + \left[ \frac{(\nu^{(m)} - \nu_{12}^{(f)})(k^{(m)} - k^{(f)})G^{(m)}}{(k^{(f)} + G^{(m)})k^{(m)} + (k^{(f)} - k^{(m)})G^{(m)}f^{(f)}} \right] f^{(f)} f^{(m)} \quad (106)$$

$$\nu_{23} = 1 - \frac{E_2}{2k_2} - 2\nu_{12}^2 \frac{E_2}{E_1} \quad (107)$$

$$G_{12} = G^{(m)} \left[ \frac{(G_{12}^{(f)} + G^{(m)}) + (G_{12}^{(f)} - G^{(m)})f^{(f)}}{(G_{12}^{(f)} + G^{(m)}) - (G_{12}^{(f)} - G^{(m)})f^{(f)}} \right] \quad (108)$$

$$G_{23} = G^{(m)} \left[ \frac{(G_{23}^{(f)} + G^{(m)})k^{(m)} + 2G_{23}^{(f)}G^{(m)} + (G_{23}^{(f)} - G^{(m)})k^{(m)}f^{(f)}}{(G_{23}^{(f)} + G^{(m)})k^{(m)} + 2G_{23}^{(f)}G^{(m)} - (G_{23}^{(f)} - G^{(m)})(k^{(m)} + 2G^{(m)})f^{(f)}} \right] \quad (109)$$

$$\alpha_1 = \frac{\alpha_1^{(f)} E_1^{(f)} + \alpha^{(m)} E^{(m)} f^{(m)}}{E_1^{(f)} f^{(f)} + E^{(m)} f^{(m)}} \quad (110)$$

$$\alpha_2 = (\alpha_2^{(f)} + \nu_{12}^{(f)} \alpha_1^{(f)}) f^{(f)} + (1 + \nu^{(m)}) \alpha^{(m)} f^{(m)} - (\nu_{12}^{(f)} f^{(f)} + \nu^{(m)} f^{(m)}) \alpha_1 \quad (111)$$

where

$$k^{(f)} = \frac{E_1^{(f)} E_2^{(f)}}{2(1 - \nu_{23}^{(f)}) E_1^{(f)} - 4(\nu_{12}^{(f)})^2 E_2^{(f)}} \quad (112)$$

$$k^{(m)} = \frac{E^{(m)}}{2(1 - \nu^{(m)}) - 4(\nu^{(m)})^2} \quad (113)$$

$$k_2 = \frac{(k^{(f)} + G^{(m)})k^{(m)} + (k^{(f)} - k^{(m)})G^{(m)}f^{(f)}}{(k^{(f)} + G^{(m)}) - (k^{(f)} - k^{(m)})f^{(f)}} \quad (114)$$

Here, superscripts  $(f)$  and  $(m)$  denote the fiber and matrix property, respectively. Subscripts 1, 2, and 3 represent the material coordinate axis of the ply shown in Figure 1.  $E$ ,  $G$ ,  $\nu$ ,  $\alpha$ ,  $k$ , and  $f$  are

**Table 8.** Material properties of E-glass fiber and resin (Malik, 2011).

Fiber Young's modulus $E^{(f)}$ (GPa)	72.4
Fiber Poisson's ratio $\nu^{(f)}$	0.2
Fiber shear modulus $G^{(f)}$ (GPa)	30.17
Fiber thermal expansion coefficient $\alpha^{(f)}$ ( $10^{-5}/^{\circ}\text{C}$ )	0.5
Fiber volume fraction $f$	0.5
Matrix Young's modulus $E^{(m)}$ (GPa)	3.4
Matrix Poisson's ratio $\nu^{(m)}$	0.35
Matrix shear modulus $G^{(m)}$ (GPa)	1.259
Matrix thermal expansion coefficient $\alpha^{(m)}$ ( $10^{-5}/^{\circ}\text{C}$ )	11.0

**Table 9.** Material properties used for calculating  $d_{11}$  (Zhao et al., 1974).

Fiber radius $r$ ( $\mu\text{m}$ )	6.5
Gauge length $L_0$ (mm)	24
Weibull modulus $m$	6.34
Fiber strength $\sigma_0$ based on $L_0$ (MPa)	1550
Fiber/matrix interfacial shear stress $\tau$ (MPa)	25

**Table 10.** Parameters of transverse crack evolution in E-glass/TX24235 GFRP  $[0/90_n/0]_s$  ( $n = 2, 4,$  and  $6$ ) laminates.

	$[0/90_2/0]_s$	$[0/90_4/0]_s$	$[0/90_6/0]_s$
$\sigma_{L0}$ (MPa)	140	70	55
$\sigma_{Lc}$ (MPa)	100	100	100
$m_T$	3.1	3.1	3.1
$\rho_s$ (mm)	21.5	16.0	10.5

the Young's modulus, shear modulus, Poisson's ratio, thermal expansion coefficient, bulk modulus, and volume fraction, respectively.  $k_2$  is the transverse plane bulk modulus.  $E_1^{(f)} = E_2^{(f)} = E^{(f)}$ ,  $G_{12}^{(f)} = G_{23}^{(f)} = G^{(f)}$ ,  $\nu_{12}^{(f)} = \nu_{23}^{(f)} = \nu^{(f)}$ , and  $\alpha_1^{(f)} = \alpha_2^{(f)} = \alpha^{(f)}$  are assumed because the E-glass fiber is isotropic. Table 8 lists the material properties of the E-glass fiber and resin used in equations (104) to (114). Tables 9 and 10 present the material properties used for calculating  $d_{11}$  and the parameters of transverse crack evolution in equation (101), respectively. The crack evolution parameters were derived by fitting the results predicted by present model with the experimental results, as shown in Figure 13(a).

Figure 13(b) shows the comparison of the stress-strain responses of E-glass/TX24235 GFRP  $[0/90_n/0]_s$  ( $n = 2, 4, 6$ ) laminates with those obtained experimentally by Okabe et al. (2004). The results predicted by the present model for the  $[0/90_2/0]_s$  laminate does not agree with the experiment results. The present model overestimated the laminate failure strength, despite considering the stiffness reduction due to transverse cracking and fiber breaks. The reason for this overestimation may be the stiffness reduction, due to additional damage modes such as delamination resulting from stress concentration at the transverse crack tip. The predicted results for  $[0/90_4/0]_s$  and  $[0/90_6/0]_s$  laminates reasonably agree with the experimental results. Furthermore, the laminate failure strength derived from the GLS model can be used to predict the results. From the results described in the previous and current sections, we concluded that the present model can reproduce the stress-strain responses of cross-ply laminates with transverse cracks and fiber breaks using the Maimí model with damage variables  $d_{11}$ ,  $d_{22}$ , and  $d_{12}$  proposed in this study.

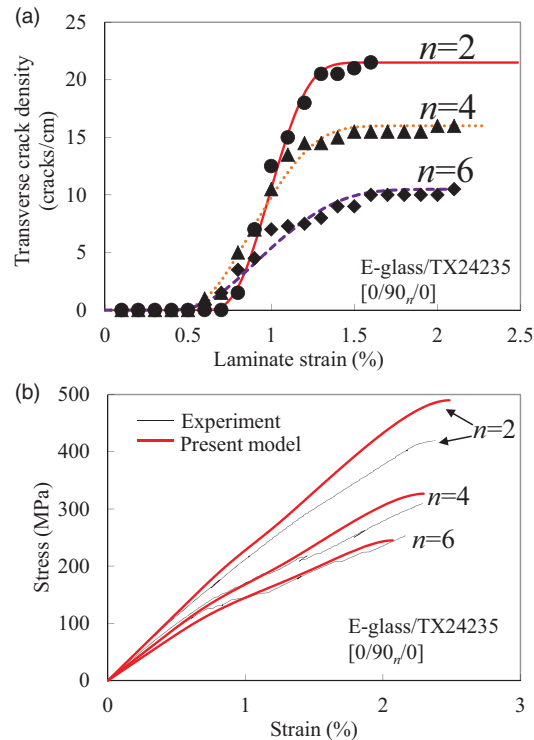


**Figure 13.** Comparison of (a) transverse cracking progression and (b) stress-strain responses of E-glass/TX24235 GFRP  $[0/90_n/0]_s$  ( $n = 2, 4, \text{ and } 6$ ) laminates predicted using the present model with experimental results (Okabe et al. (2004)).

## Conclusions

This study involved deriving a new analytical model for predicting the effective compliance of composite laminates and simplified expressions for the damage tensor. We evaluated four models that yielded asymmetric/symmetric compliance matrices of damaged composite plies. Damage variable  $d_{11}$  describing stiffness reduction due to fiber breaks and its upper bound  $d_{11}^{\max}$  given by  $1/(m+2)$  were formulated using the GLS model. Moreover, the simplified analytical forms of damage variables  $d_{22}$  and  $d_{12}$  were developed, assuming that the displacement field along the longitudinal direction could be expressed as a quadric function by loosening the boundary condition for the governing differential equation. We also proved that the effective laminate properties could be obtained by substituting the damage variables into the CLT- and CDM-based models. Comparisons of the effective stiffness of laminates with transverse cracking to the results obtained via finite element calculations were performed for model verification. We found that the Maimí model (Maimí et al., 2007) in combination with the proposed formulation for the damage variables, referred to as Maimí\_simplified in this study, was the most appropriate model for predicting or estimating damage in composite laminates with transverse cracking.

The nonlinear stress-strain behaviors of CFRP cross-ply laminates resulting from transverse cracking were predicted using the present model, and the predicted results are compared with the experimental results. The effective compliance model with simplified damage variable  $d_{22}$  and  $d_{12}$

was utilized to calculate the stiffness reduction of the CFRP laminates. The ultimate tensile strength of CFRP cross-ply laminates was predicted based on a strain-based fiber failure criterion because fiber fracture in CFRP laminate occurs at the ultimate laminate failure stress. We assumed that the laminate failed when the effective axial laminate strain became equal to the ultimate fiber axial failure strain in  $0^\circ$  plies. The ultimate fiber axial failure strain was derived from SEM simulations. The present model quantitatively reproduced the experimental results up to the ultimate failure strength of the laminate.

We predicted the nonlinear stress–strain behavior of  $[0/90_n/0]_s$  ( $n = 2, 4, 6$ ) GFRP cross-ply laminates with transverse cracks in  $90^\circ$  plies and fiber breaks in  $0^\circ$  plies to validate our proposed damage tensor  $d_{11}$ ,  $d_{22}$ , and  $d_{12}$ .  $d_{11}$  associated with fiber breaks and its upper bound describing the ultimate failure condition were analytically derived using the GLS model (Curtin, 1991). The effective stiffness model with simple damage variables  $d_{11}$ ,  $d_{22}$ , and  $d_{12}$  was utilized to evaluate the stiffness reduction due to transverse cracking, fiber breaks, and ultimate failure of the laminate. In  $[0/90_4/0]_s$  and  $[0/90_6/0]_s$  laminates, the results predicted using the developed model showed reasonable agreement with the experimental results when the transverse cracking progression was fitted with the experimental results. Thus, if transverse cracking progression is formulated properly, the stress–strain diagram can be reproduced better.

### Acknowledgements

We would like to thank S Date (Tohoku University) for his support in conducting the SEM simulations. We would also like to express our appreciation to S Kochii (Tohoku University) for his assistance while performing experiments. The authors would like to thank Editage (www.editage.com) for English language editing.

### Declaration of conflicting interests

The author(s) declared no potential conflicts of interest with respect to the research, authorship, and/or publication of this article.

### Funding

The author(s) disclosed receipt of the following financial support for the research, authorship, and/or publication of this article: The authors disclosed receipt of the following financial support for the research, authorship, and/or publication: Council for Science, Technology and Innovation (CSTI), Cross-ministerial Strategic Innovation Promotion Program (SIP), “Materials Integration” for revolutionary design system of structural materials (Funding agency: JST); University of Washington-Tohoku University: Academic Open Space (UW-TU: AOS); Toray Industries, Inc.; JSPS KAKENHI Grant No. JP 18J20899.

### ORCID iD

Sota Onodera  <https://orcid.org/0000-0002-1313-2921>

### References

- Allen D, Harris C and Groves S (1987a) A thermomechanical constitutive theory for elastic composites with distributed damage-I. Theoretical development. *International Journal of Solids and Structures* 23(9): 1301–1318.
- Allen D, Harris C and Groves S (1987b) A thermomechanical constitutive theory for elastic composites with distributed damage-II. Application to matrix cracking in laminated composites. *International Journal of Solids and Structures* 23(9): 1319–1338.

- Bailey JE and Parvizi A (1981) On fibre debonding effects and the mechanism of transverse-ply failure in cross-ply laminates of glass fibre/thermoset composites. *Journal of Materials Science* 16(3): 649–659.
- Cox HL (1952) The elasticity and strength of paper and other fibrous materials. *British Journal of Applied Physics* 3(3): 72–79.
- Curtin WA (1991a) Exact theory of fibre fragmentation in a single-filament composite. *Journal of Materials Science* 26(19): 5239–5253.
- Curtin WA (1991b) Theory of mechanical properties of ceramic-matrix composites. *Journal of the American Ceramic Society* 74(11): 2837–2845.
- Dvorak GJ and Laws N (1987) Analysis of progressive matrix cracking in composite laminates II. First ply failure. *Journal of Composite Materials* 21(4): 309–329.
- Dvorak GJ, Laws N and Hejazi M (1985) Analysis of progressive matrix cracking in composite laminates I. Thermoelastic properties of a ply with cracks. *Journal of Composite Materials* 19(3): 216–234.
- Fikry MM, Ogihara S and Vinogradov V (2018) The effect of matrix cracking on mechanical properties in FRP laminates. *Mechanics of Advanced Materials and Modern Processes* 4(1): 3.
- Garrett KW and Bailey JE (1977a) Multiple transverse fracture in 90° cross-ply laminates of a glass fibre-reinforced polyester. *Journal of Materials Science* 12(1): 157–168.
- Garrett KW and Bailey JE (1977b) The effect of resin failure strain on the tensile properties of glass fibre-reinforced polyester cross-ply laminates. *Journal of Materials Science* 12(11): 2189–2194.
- Gudmundson P and Zang W (1993) An analytic model for thermoelastic properties of composite laminates containing transverse matrix cracks. *International Journal of Solids and Structures* 30(23): 3211–3231.
- Hajikazemi M and McCartney LN (2018) Comparison of variational and generalized plane strain approaches for matrix cracking in general symmetric laminates. *International Journal of Damage Mechanics* 27(4): 507–540.
- Han Y, Hahn H and Croman R (1988) A simplified analysis of transverse ply cracking in cross-ply laminates. *Composites Science and Technology* 31(3): 165–177.
- Hashin Z (1986) Analysis of stiffness reduction of cracked cross-ply laminates. *Engineering Fracture Mechanics* 25(5–6): 771–778.
- Hashin Z (1987) Analysis of orthogonally cracked laminates under tension. *Journal of Applied Mechanics* 54(4): 872–879.
- Hui CY, Phoenix S, Ibnabdeljalil M, et al. (1995) An exact closed form solution for fragmentation of Weibull fibers in a single filament composite with applications to fiber-reinforced ceramics. *Journal of the Mechanics and Physics of Solids* 43(10): 1551–1585.
- Ibnabdeljalil M and Curtin W (1997) Strength and reliability of fiber-reinforced composites: Localized load-sharing and associated size effects. *International Journal of Solids and Structures* 34(21): 2649–2668.
- Kanagawa Y, Murakami S, Liu Y, et al. (1996) Description of internal damage in FRP laminates by continuum damage mechanics. *Journal of the Society of Materials Science, Japan* 45(2): 206–211.
- Kobayashi S, Ogihara S and Takeda N (2000) Damage mechanics analysis for predicting mechanical behavior of general composite laminates containing transverse cracks. *Advanced Composite Materials* 9(4): 363–375.
- Kravchenko OG, Kravchenko SG and Pipes RB (2017) Cure history dependence of residual deformation in a thermosetting laminate. *Composites Part A: Applied Science and Manufacturing* 99: 186–197.
- Kumagai Y, Onodera S, Salviato M, et al. (2020) Multiscale analysis and experimental validation of crack initiation in quasi-isotropic laminates. *International Journal of Solids and Structures* 193–194: 172–191.
- Lee JW, Allen D and Harris C (1989) Internal state variable approach for predicting stiffness reductions in fibrous laminated composites with matrix cracks. *Journal of Composite Materials* 23(12): 1273–1291.
- Lee JW and Daniel I (1990) Progressive transverse cracking of crossply composite laminates. *Journal of Composite Materials* 24(11): 1225–1243.
- Li S, Wang M, Jeanmeure L, et al. (2019) Damage related material constants in continuum damage mechanics for unidirectional composites with matrix cracks. *International Journal of Damage Mechanics* 28(5): 690–707.

- McCartney LN (1992) Theory of stress transfer in a  $0$ - $90$ - $0$  cross-ply laminate containing a parallel array of transverse cracks. *Journal of the Mechanics and Physics of Solids* 40(1): 27–68.
- McCartney L (2005) Energy-based prediction of progressive ply cracking and strength of general symmetric laminates using an homogenisation method. *Composites Part A: Applied Science and Manufacturing* 36(2): 119–128.
- Maimí P, Camanho P, Mayugo J, et al. (2007) A continuum damage model for composite laminates: Part I – Constitutive model. *Mechanics of Materials* 39(10): 897–908.
- Malik SA (2011) *Damage detection using self-sensing composites*. PhD Thesis, University of Birmingham, UK.
- Manders PW, Chou TW, Jones FR, et al. (1983) Statistical analysis of multiple fracture in  $0/90/0$  glass fibre/epoxy resin laminates. *Journal of Materials Science* 18(10): 2876–2889.
- Murakami S (2012) *Continuum Damage Mechanics, Solid Mechanics and Its Applications*. vol. 185. Dordrecht, The Netherlands: Springer.
- Nairn JA and Hu S (1992) The initiation and growth of delaminations induced by matrix microcracks in laminated composites. *International Journal of Fracture* 57(1): 1–24.
- Neumeister JM (1993) A constitutive law for continuous fiber reinforced brittle matrix composites with fiber fragmentation and stress recovery. *Journal of the Mechanics and Physics of Solids* 41(8): 1383–1404.
- Noda J, Okabe T, Takeda N, et al. (2004) Damage process of GFRP cross-ply laminates. *Transactions of the Japan Society of Mechanical Engineers Series A* 70(698): 1364–1369.
- Okabe T, Imamura H, Sato Y, et al. (2015) Experimental and numerical studies of initial cracking in CFRP cross-ply laminates. *Composites Part A: Applied Science and Manufacturing* 68: 81–89.
- Okabe T, Onodera S, Kumagai Y, et al. (2018) Continuum damage mechanics modeling of composite laminates including transverse cracks. *International Journal of Damage Mechanics* 2018; 27(6): 877–895.
- Okabe T, Sekine H, Ishii K, et al. (2005) Numerical method for failure simulation of unidirectional fiber-reinforced composites with spring element model. *Composites Science and Technology* 65(6): 921–933.
- Okabe T, Sekine H, Noda J, et al. (2004) Characterization of tensile damage and strength in GFRP cross-ply laminates. *Materials Science and Engineering A* 383(2): 381–389.
- Onodera S and Okabe T (2019) Three-dimensional analytical model for effective elastic constants of transversely isotropic plates with multiple cracks: Application to stiffness reduction and steady-state cracking of composite laminates. *Engineering Fracture Mechanics* 219: 106595.
- Pagano N, Schoeppner G, Kim R, et al. (1998) Steady-state cracking and edge effects in thermo-mechanical transverse cracking of cross-ply laminates. *Composites Science and Technology* 58(11): 1811–1825.
- Parvizi A and Bailey JE (1978) On multiple transverse cracking in glass fibre epoxy cross-ply laminates. *Journal of Materials Science* 13(10): 2131–2136.
- Parvizi A, Garrett KW and Bailey JE (1978) Constrained cracking in glass fibre-reinforced epoxy cross-ply laminates. *Journal of Materials Science* 13(1): 195–201.
- Rosen BW (1964) Tensile failure of fibrous composites. *AIAA Journal* 2(11): 1985–1991.
- Talreja R (1985) A continuum mechanics characterization of damage in composite materials. *Proceedings of the Royal Society A: Mathematical, Physical and Engineering Sciences* 399: 195–216.
- Vinogradov V and Hashin Z (2010) Variational analysis of cracked angle-ply laminates. *Composite Science Technology* 70(4): 638–646.
- Wang A, Chou P and Lei S (1984) A stochastic model for the growth of matrix cracks in composite laminates. *Journal of Composite Materials* 18(3): 239–254.
- Xia Z, Carr R and Hutchinson J (1993) Transverse cracking in fiber-reinforced brittle matrix, cross-ply laminates. *Acta Metallurgica Materials* 41(8): 2365–2376.
- Yamamoto G, Onodera M, Koizumi K, et al. (2019) Considering the stress concentration of fiber surfaces in the prediction of the tensile strength of unidirectional carbon fiber-reinforced plastic composites. *Composites Part A: Applied Science and Manufacturing* 121: 499–509.
- Yoshimura A, Okabe T, Yamada M, et al. (2011) Damage simulation of CFRP laminates under high velocity projectile impact. In: *18th International conference on composites materials*, Jeju, South Korea, 21–26 August.
- Zhao FM, Okabe T and Takeda N (2000) The estimation of statistical fiber strength by fragmentation tests of single-fiber composites. *Composites Science Technology* 60(10): 1965–1974.